Diphosphene and Diphosphinylidene†

Tongxiang Lu, Andrew C. Simmonett, Francesco A. Evangelista, Yukio Yamaguchi, and Henry F. Schaefer III*

Center for Computational Quantum Chemistry, University of Georgia, Athens, Georgia 30602

Received: April 30, 2009; Revised Manuscript Received: June 22, 2009

The equilibrium structures of P_2H_2 isomers and the associated isomerization transition states have been investigated systematically starting from self-consistent-field theory and proceeding to coupled cluster methods using a wide range of basis sets. For each structure, the geometry, energy, dipole moment, harmonic vibrational frequencies, and infrared intensities have been predicted. The global minimum has been confirmed to be planar trans-HPPH diphosphene, lying 3.2 kcal mol^{-1} below cis-HPPH with the aug-cc-pVQZ CCSD(T) method upon inclusion of zero-point vibrational energy corrections. Diphosphinylidene, which has the connectivity PPH_2 and C_{2v} symmetry, lies 25.2 kcal mol^{-1} above the global minimum. The trans-cis isomerization reaction occurs via internal rotation with a barrier of 35.2 kcal mol^{-1} using the cc-pVQZ Mk-MRCCSD (2e/2MO) method. This transition state exhibits multireference character and consequently properties were evaluated using CASSCF, MRCI, CASPT2, and Mk-MRCCSD methods with various basis sets. At the aug-cc-pVQZ CCSD(T) level, the transition state for the isomerization reaction between trans-HPPH and diphosphinylidene (planar PPH_2) is predicted to be nonplanar with a torsional angle of 101.1°. The corresponding barrier is estimated to be 48.2 kcal mol^{-1}.

Introduction

Heavier main group elements with low coordination numbers have attracted much attention over the last two decades.[1−7] The interest in such compounds stems from their reactivity toward a diverse range of chemical reagents and their unique electrochemical and photochemical properties.[1,8−12] More recent research suggests that secondary diphosphines and diphosphenes (HPPH) are potential candidates for use in chemical hydrogen storage systems.[13]

In the absence of steric factors, these small phosphorus compounds with low coordination numbers often tend to form oligomers due to thermodynamic preferences.[14] The preparation of the first stable diphophene was reported in 1981 by Yoshifuji and co-workers,[15] who used sterically bulky substituents (RP═PR, R = 2,4,6-tritert-butylphenyl) to achieve kinetic stability. Since then, the synthesis, structure, and reactivity of various doubly bonded phosphorus compounds have been examined, typically employing bulky ligands to ensure stability.[6,16−22] More recently, a carbene stabilized diphosphorus compound was synthesized in which the phosphorus behaves as an electron acceptor.[22] The geometries of several diphosphenes have been determined using X-ray crystallographic analyses.[23] The PP bond length varies in the range of 2.001 to 2.034 Å, which shows that the PP bond has double-bond character.[24] The large difference between the bond angles of TbtP═PTbt (Tbt = 2,4,6-tris[bis(trimethylsilyl)-methyl]phenyl) (106.4 and 104.5°) and the ideal sp^2 hybridized bond angle (120°) may be caused by the lower tendency of second row or higher atoms to form hybridized orbitals.[12,20] The activation free energy for the trans-cis conversion of Mes*PPMes* (2,4,6-tri-tert-butylphenyl or supermesityl) was deduced to be 20.3 kcal mol^{-1} at 0 °C through laser irradiation.[25] Moreover, the vibrational frequency of PP stretching of Mes*PPMes* was determined to be 610 cm^{-1} from Raman spectra.[26]

In order to further understand these small phosphorus compounds with low coordination numbers, theoretical investigations of their bonding and reactivity have been performed using simplified model systems as prototypes.[27−36] Theoretical calculations have shown that the singlet state of diphosphinylidene is stabilized via implantation of alkyl and/or amino groups at the β-position due to π-donating and steric effects. Moreover, bulky substituents destabilize the triplet state.[37] Furthermore, it has been demonstrated that the triplet state of PPF_2 lies below the singlet state, in contrast to PPHCl and PPHF whose ground states are singlets.[38] Diphosphene has a larger singlet−triplet separation of about 1.2 eV,[28] which is relatively small compared to the first-row isolobal HNNH molecule (2 eV)[39] or the triply bonded HCCH molecule (3.5 eV).[40]

In the present research, we investigate the prototypical doubly bonded phosphorus systems by characterizing the closed-shell structures of diphosphene (HPPH) and diphosphinylidene (PPH_2) using high-accuracy ab initio methods in concert with large Gaussian basis sets; these structures are depicted in Figure 1. Special emphasis is placed on the analysis of the isomerization transition state between trans- and cis-HPPH diphosphene structures. The latter system requires multireference theoretical treatments. Finally, the transition state for the isomerization reaction between trans-HPPH and diphosphinylidene, which involves a hydrogen migration, is investigated. For brevity, we shall hereafter refer to diphoshinylidene simply as planar PPH_2.

Electronic Structure Considerations

In previous theoretical studies, the electronic ground state of the diphosphene molecule was found[28] to have a C_{2h}-symmetric trans-HPPH structure with an electron configuration of

$$[(\text{core})(5a_g)^2(5b_u)^2(6b_u)^2(6a_g)^2(7a_g)^2(2a_u)^2]$$

where (core) denotes the ten lowest-lying core orbitals (P:1s, 2s, 2p-like). The $2a_u$ molecular orbital is the highest occupied

† Part of the "Robert W. Field Festschrift".

* To whom correspondence should be addressed. E-mail: sch@uga.edu.

10.1021/jp904028a CCC: $40.75
Published on Web 07/13/2009

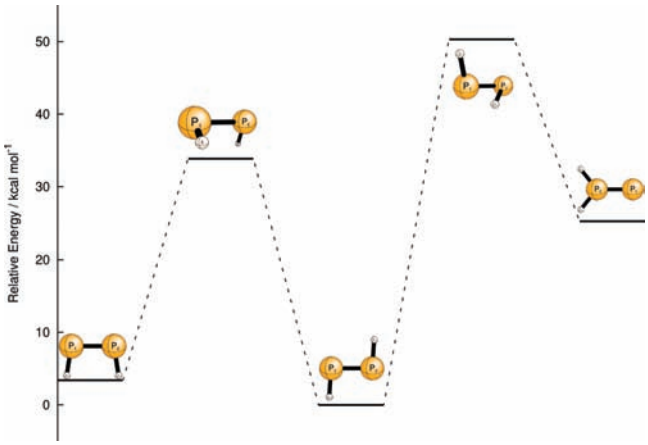

Figure 1. Schematic potential energy surface showing cis-HPPH (left), trans-HPPH (center), planar PPH_2 (right), and two isomerization transition states connecting them.

molecular orbital (HOMO), while the $2b_g$ molecular orbital represents the lowest unoccupied molecular orbital (LUMO), as shown in Figure 7. A C_{2v}-symmetric cis-isomer, with an electron configuration of

$$[(\text{core})(5a_1)^2(5b_2)^2(6a_1)^2(7a_1)^2(6b_2)^2(2b_1)^2]$$

is also located on the lowest closed-shell singlet surface. The $2b_1$ molecular orbital (HOMO), which is depicted in Figure 8a, represents the bonding π orbital; the $2a_2$ orbital (LUMO) in Figure 8b represents the antibonding π-orbital.

On the same closed shell singlet surface there exists another isomer of vinylidene type, the C_{2v}-symmetric diphosphinylidene (PPH_2) molecule. The latter's frontier orbitals are illustrated in Figure 9. The electron configuration of PPH_2 may be described as

$$[(\text{core})(7a_1)^2(8a_1)^2(3b_2)^2(9a_1)^2(3b_1)^2(4b_2)^2]$$

The C_2 symmetric transition state for the isomerization reaction of trans- to cis-HPPH via rotation about the H−P−P−H torsional angle is minimally represented by a linear combination of the electron configurations

$$[(\text{core})(6a)^2(6b)^2(7a)^2(7b)^2(8a)^2(9a)^2]$$

and

$$[(\text{core})(6a)^2(6b)^2(7a)^2(7b)^2(8a)^2(8b)^2]$$

and therefore requires multideterminant methods to be described correctly. Moreover, active space orbitals are shown in Figure 10. Finally the transition state for an isomerization reaction between trans-HPPH and planar PPH_2 possesses the following electronic configuration

$$[(\text{core})(11a)^2(12a)^2(13a)^2(14a)^2(15a)^2(16a)^2]$$

the HOMO and LUMO are demonstrated in Figure 11.

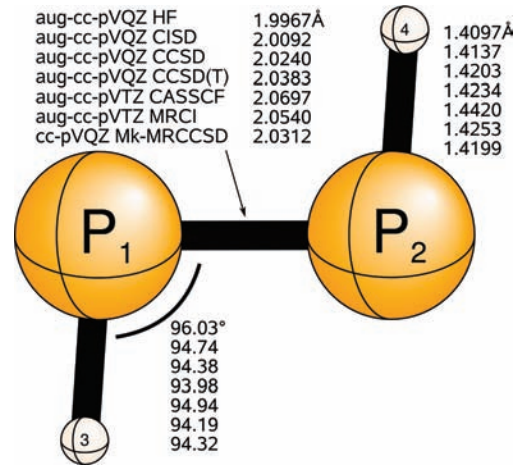

Figure 2. Theoretical geometries for trans-HPPH.

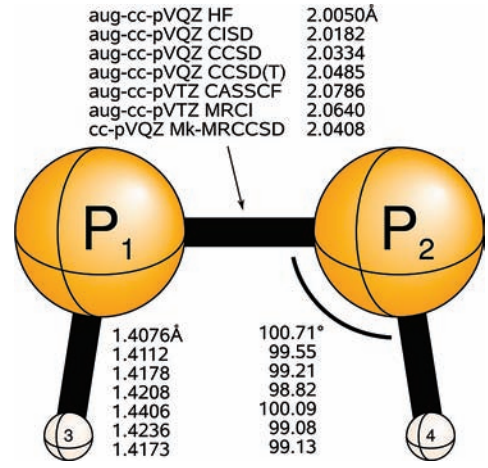

Figure 3. Theoretical geometries for cis-HPPH.

Theoretical Procedures

In this research, the correlation-consistent family of basis sets cc-pVXZ (X = D, T, and Q) and aug-cc-pV*X*Z (X = D, T, and Q) developed by Dunning and co-workers was used.[41,42] The zeroth-order description was obtained using one-configuration restricted close-shell Hartree−Fock (RHF) wave functions. The effects of electron correlation were systematically explored using configuration interaction with single and double excitations (CISD),[43−45] coupled cluster with single and double excitations (CCSD),[46,47] CCSD with

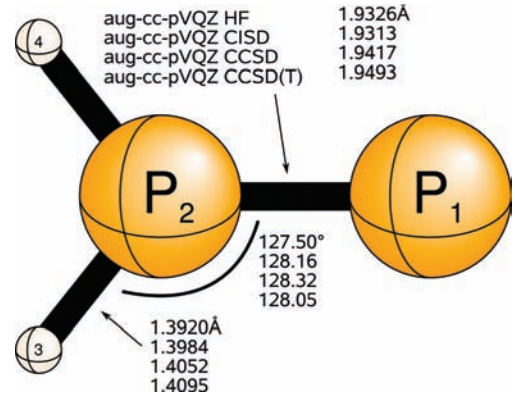

Figure 4. Theoretical geometries for planar PPH_2.

TABLE 1: Theoretical Prediction of Harmonic Vibrational Frequencies (in cm^{-1}), Infrared Intensities (in Parentheses in km mol^{-1}), and ZPVE (in kcal mol^{-1}) for the ^1A_g trans-HPPH Molecule

theory	$\omega_1(a_g)$	$\omega_2(a_g)$	$\omega_3(a_g)$	$\omega_4(a_u)$	$\omega_5(b_u)$	$\omega_6(b_u)$	ZPVE
aug-cc-pVTZ HF	2493	1045	696	849	2509 (128.3)	736 (17.4)	11.91
aug-cc-pVQZ HF	2495	1048	698	852	2511 (126.7)	737 (17.7)	11.92
cc-pVTZ CISD[a]	2438	1001	659	811	2453	697	11.52
cc-pVQZ CISD	2446	1005	667	814	2461	701	11.57
aug-cc-pVTZ CISD	2437	999	658	807	2452	699	11.51
aug-cc-pVQZ CISD	2445	1004	666	813	2460	702	11.57
cc-pVTZ CCSD	2382	978	629	782	2396 (113.9)	683 (10.8)	11.22
cc-pVQZ CCSD	2390	983	638	787	2405 (99.3)	688 (11.7)	11.28
aug-cc-pVTZ CCSD	2379	977	628	778	2394 (103.0)	685 (12.0)	11.21
aug-cc-pVQZ CCSD	2388	982	637	785	2403 (96.4)	689 (12.3)	11.28
cc-pVTZ CCSD(T)	2358	963	601	762	2373 (110.4)	671 (10.0)	11.05
cc-pVQZ CCSD(T)	2366	968	611	767	2381 (95.6)	676 (10.8)	11.11
aug-cc-pVTZ CCSD(T)	2354	961	599	758	2370 (100.4)	673 (11.1)	11.03
aug-cc-pVQZ CCSD(T)	2363	967	610	765	2379 (93.4)	677 (11.2)	11.10
cc-pVDZ CASSCF[b]	2243	956	568	746	2260 (178.3)	672 (10.1)	10.64
cc-pVTZ CASSCF	2237	958	578	752	2256 (150.6)	668 (11.1)	10.65
aug-cc-pVDZ CASSCF	2242	951	568	738	2259 (139.9)	669 (11.5)	10.62
aug-cc-pVTZ CASSCF	2241	956	578	751	2259 (135.5)	668 (13.0)	10.65
cc-pVDZ MRCI	2340	964	576	749	2356 (158.9)	674 (9.8)	10.95
cc-pVTZ MRCI	2331	969	594	761	2352 (121.7)	665 (11.4)	10.97
aug-cc-pVDZ MRCI	2324	955	572	733	2340 (126.5)	669 (11.7)	10.86
aug-cc-pVTZ MRCI	2329	967	593	758	2350 (110.0)	666 (12.8)	10.96

[a] The algorithm used to compute the CISD energies did not afford dipole moments or derivatives thereof. [b] The active space is defined as (12e/10MO).

perturbative triple excitations [CCSD(T)],[48−50] complete active space self-consistent-field (CASSCF),[51,52] internally contracted multireference CI (MRCI)[53,54](based on the CASSCF reference), CAS second-order perturbation theory (CASPT2),[55−57] and the state-specific multireference coupled cluster approach suggested by Mukherjee and co-workers (Mk-MRCCSD).[58−60] For Mk-MRCCSD calculations, two-configuration SCF (TCSCF) orbitals were employed. The active space orbitals were canonicalized by transforming to the natural orbital basis. In the correlated procedures the ten lowest-lying core orbitals (P:1s, 2s, 2p- like) were frozen, in keeping with the design of the basis sets used. At the SCF, CCSD, and CCSD(T) levels of theory, geometries, harmonic vibrational frequencies, and infrared (IR) intensities were obtained using analytic derivative methods, while at the CISD, CASSCF, MRCI, CASPT2, and Mk-MRCCSD levels of theory numerical differentiation was used. For trans-HPPH, cis-HPPH, and the isomerization transition state between them, the number of configuration state functions (CSFs) are 3620, 3620, and 13860, respectively, at the (12e/10MO) CASSCF level of theory. The computations were carried out using the Molpro,[61] MAB-AcesII,[62,63] and Psi3[64] ab initio quantum chemistry packages. The Mk-MRCCSD calculations were performed with the Psi3 and MCSCF codes.[65,66]

TABLE 2: Theoretical Prediction of Harmonic Vibrational Frequencies (in cm^{-1}), Infrared Intensities (in Parentheses in km mol^{-1}), ZPVE (in kcal mol^{-1}), and Dipole Moments (μ_e, in Debye) for the $^1A_1$ cis-HPPH Molecule

theory	μ_e	$\omega_1(a_1)$	$\omega_2(a_1)$	$\omega_3(a_1)$	$\omega_4(a_2)$	$\omega_5(b_2)$	$\omega_6(b_2)$	ZPVE
aug-cc-pVTZ HF	1.347	2522 (95.0)	806 (21.6)	690 (1.2)	769	2497 (28.4)	935 (12.6)	11.75
aug-cc-pVQZ HF	1.342	2525 (93.7)	808 (21.9)	692 (1.2)	771	2499 (28.4)	937 (13.3)	11.77
cc-pVTZ CISD[a]		2468	765	649	730	2443	881	11.35
cc-pVQZ CISD		2477	772	657	732	2452	884	11.40
aug-cc-pVTZ CISD		2467	769	647	725	2442	878	11.33
aug-cc-pVQZ CISD		2475	773	656	732	2451	883	11.39
cc-pVTZ CCSD	1.134	2411 (87.2)	747 (13.7)	618 (1.4)	702	2387 (18.0)	859 (15.5)	11.04
cc-pVQZ CCSD	1.146	2420 (75.7)	755 (14.5)	627 (1.7)	705	2396 (16.2)	862 (16.9)	11.10
aug-cc-pVTZ CCSD	1.102	2408 (79.5)	751 (14.6)	616 (1.8)	698	2383 (15.6)	855 (16.8)	11.03
aug-cc-pVQZ CCSD	1.128	2417 (74.0)	756 (14.9)	626 (1.8)	705	2393 (15.5)	861 (17.1)	11.09
cc-pVTZ CCSD(T)	1.106	2387 (85.6)	731 (12.5)	587 (1.5)	681	2364 (15.9)	839 (16.4)	10.85
cc-pVQZ CCSD(T)	1.115	2395 (73.5)	740 (13.2)	598 (1.7)	685	2372 (14.4)	842 (17.7)	10.91
aug-cc-pVTZ CCSD(T)	1.065	2383 (78.3)	737 (13.3)	586 (1.9)	677	2359 (13.9)	836 (17.4)	10.83
aug-cc-pVQZ CCSD(T)	1.092	2392 (72.3)	741 (13.5)	597 (1.9)	685	2369 (13.8)	842 (17.8)	10.90
cc-pVDZ CASSCF[b]	1.307	2265 (137.6)	729 (12.3)	556 (0.9)	673	2239 (31.6)	851 (16.5)	10.45
cc-pVTZ CASSCF	1.232	2264 (117.1)	724 (12.7)	567 (1.2)	679	2235 (25.8)	845 (17.9)	10.46
aug-cc-pVDZ CASSCF	1.243	2266 (111.3)	730 (13.0)	556 (1.3)	669	2240 (23.2)	842 (18.2)	10.44
aug-cc-pVTZ CASSCF	1.234	2267 (106.6)	725 (14.0)	566 (1.5)	677	2238 (22.8)	843 (19.9)	10.46
cc-pVDZ MRCI	1.188	2365 (125.4)	736 (11.8)	563(1.1)	670	2340 (22.2)	848 (18.0)	10.75
cc-pVTZ MRCI	1.156	2367 (95.9)	728 (12.9)	581(1.5)	680	2337 (17.4)	838 (18.2)	10.76
aug-cc-pVDZ MRCI	1.092	2352 (101.7)	734 (13.1)	559 (1.7)	650	2326 (16.4)	828 (19.2)	10.65
aug-cc-pVTZ MRCI	1.134	2365 (87.7)	732 (13.9)	580 (1.8)	676	2334 (15.1)	834 (19.9)	10.75

[a] The algorithm used to compute the CISD energies did not afford dipole moments or derivatives thereof. [b] The active space is defined as (12e/10MO).

Results and Discussion

Energy Minima. Selected optimized geometrical parameters for the minimum energy structures are reported in Figure 2−Figure 4. Harmonic vibrational frequencies and physical properties for trans-HPPH, cis-HPPH, and PPH_2 are given in Table 1, Table 2, and Table 3, respectively, while total energies and relative energies for these structures are presented in Table 4.

In order to correctly capture the multireference character of the isomerization transition state between the trans and cis structures, the (12e/10MO) CASSCF and MRCI wave functions of these closed-shell structures were constructed using a variety of basis sets. This active space spans the full valence space of the orbitals and electrons in the constituent atoms. For the trans isomer, the aug-cc-pVTZ CASSCF wave function is written in terms of natural orbitals as

$$\begin{aligned}\Psi = {} & 0.945\Phi_1[(\text{core})(5a_g)^2(5b_u)^2(6b_u)^2(6a_g)^2(7a_g)^2(2a_u)^2] \\ & - 0.207\Phi_2[(\text{core})(5a_g)^2(5b_u)^2(6b_u)^2(6a_g)^2(7a_g)^2(2b_g)^2] \\ & - 0.055\Phi_3[(\text{core})(5a_g)^2(5b_u)^2(6b_u)^2(6a_g)^2(2a_u)^2(7b_u)^2] \\ & - 0.053\Phi_4[(\text{core})(5a_g)^2(5b_u)^2(6b_u)^2(6a_g)^2(7a_g\alpha)(2a_u\beta) \\ & \qquad (2b_g\alpha)(7b_u\beta)] \\ & - 0.051\Phi_5[(\text{core})(5a_g)^2(5b_u)^2(6b_u)^2(6a_g)^2(7a_g\beta)(2a_u\alpha) \\ & \qquad (2b_g\beta)(7b_u\alpha)] \\ & + \text{.....}\end{aligned}$$

The analogous aug-cc-pVTZ MRCI wavefunction is described, in terms of natural orbitals, by

TABLE 3: Theoretical Prediction of Harmonic Vibrational Frequencies (in cm^{-1}), Infrared Intensities (in Parentheses in km mol^{-1}), ZPVE (in kcal mol^{-1}), and Dipole Moments (μ_e, in Debye) for the $^1A_1$ Planar PPH_2 Structure

theory	μ_e	$\omega_1(a_1)$	$\omega_2(a_1)$	$\omega_3(a_1)$	$\omega_4(b_1)$	$\omega_5(b_2)$	$\omega_6(b_2)$	ZPVE
aug-cc-pVTZ HF	2.460	2590 (32.0)	1228 (66.9)	707 (2.9)	367 (46.6)	2595 (22.6)	700 (0.0)	11.71
aug-cc-pVQZ HF	2.455	2592 (33.4)	1234 (68.5)	712 (2.5)	379 (45.6)	2596 (22.6)	707 (0.0)	11.75
cc-pVTZ CISD[a]		2513	1200	712	407	2514	667	9.45
cc-pVQZ CISD		2519	1199	720	415	2520	672	9.50
aug-cc-pVTZ CISD		2512	1190	709	403	2515	660	9.43
aug-cc-pVQZ CISD		2517	1196	719	414	2518	671	9.50
cc-pVTZ CCSD	2.226	2451 (46.9)	1180 (80.1)	694 (0.0)	387 (23.3)	2452 (49.5)	644 (0.3)	11.16
cc-pVQZ CCSD	2.276	2457 (45.5)	1177 (77.3)	702 (0.0)	392 (24.7)	2458 (35.7)	651 (0.7)	11.20
aug-cc-pVTZ CCSD	2.276	2450 (47.9)	1168 (77.0)	690 (0.0)	382 (26.9)	2452 (32.9)	639 (1.2)	11.12
aug-cc-pVQZ CCSD	2.288	2455 (46.7)	1173 (76.7)	701 (0.0)	391 (26.7)	2456 (30.4)	649 (1.2)	11.19
cc-pVTZ CCSD(T)	2.211	2415 (56.1)	1173 (87.0)	681 (0.0)	394 (20.4)	2412 (56.7)	630 (0.8)	11.01
cc-pVQZ CCSD(T)	2.258	2418 (53.9)	1168 (83.5)	689 (0.0)	397 (21.8)	2420 (40.9)	636 (1.3)	11.05
aug-cc-pVTZ CCSD(T)	2.262	2412 (57.5)	1159 (83.7)	676 (0.0)	388 (23.7)	2412 (38.1)	624 (2.1)	10.97
aug-cc-pVQZ CCSD(T)	2.271	2417 (55.5)	1164 (82.9)	687 (0.0)	395 (23.5)	2417 (34.9)	633 (2.0)	11.03

[a] The algorithm used to compute the CISD energies did not afford dipole moments or derivatives thereof.

TABLE 4: Theoretical Predictions of the Total Energies (in E_h) for the Three Structures (Relative Energies (ΔE_e) and ZPVE-Corrected Relative Energies (ΔE_0) are in kcal mol^{-1} With Respect to the trans-HPPH Closed-Shell Structure Obtained by the Same Method and Basis Set)

	^1A_g trans-HPPH	$^1A_1$ cis-HPPH			$^1A_1$ planar PPH_2		
theory	energy	energy	ΔE_e	ΔE_0	energy	ΔE_e	ΔE_0
aug-cc-pVTZ HF	−682.643184	−682.637648	3.47	3.32	−682.604043	24.56	24.36
aug-cc-pVQZ HF	−682.650899	−682.645323	3.50	3.34	−682.612349	24.19	24.02
cc-pVTZ CISD	−682.936526	−682.931052	3.43	3.26	−682.895999	25.43	23.37
cc-pVQZ CISD	−682.960652	−682.955068	3.50	3.33	−682.921286	24.70	22.63
aug-cc-pVTZ CISD	−682.941826	−682.936285	3.48	3.30	−682.901282	25.44	23.37
aug-cc-pVQZ CISD	−682.962771	−682.957158	3.52	3.35	−682.923366	24.73	22.65
cc-pVTZ CCSD	−682.972302	−682.967008	3.32	3.14	−682.930975	25.93	25.87
cc-pVQZ CCSD	−682.998244	−682.992861	3.38	3.19	−682.958224	25.11	25.03
aug-cc-pVTZ CCSD	−682.978383	−682.973065	3.34	3.15	−682.937109	25.90	25.81
aug-cc-pVQZ CCSD	−683.000584	−682.995192	3.38	3.20	−682.960555	25.12	25.03
cc-pVTZ CCSD(T)	−682.991391	−682.986079	3.33	3.14	−682.949601	26.22	26.19
cc-pVQZ CCSD(T)	−683.019299	−683.013909	3.38	3.19	−682.979005	25.28	25.23
aug-cc-pVTZ CCSD(T)	−682.998344	−682.993045	3.32	3.13	−682.956710	26.13	26.06
aug-cc-pVQZ CCSD(T)	−683.021992	−683.016610	3.38	3.18	−682.981711	25.28	25.21
cc-pVDZ CASSCF[a]	−682.704374	−682.699485	3.07	2.88			
cc-pVTZ CASSCF	−682.730516	−682.725698	3.02	2.83			
aug-cc-pVDZ CASSCF	−682.708350	−682.703552	3.01	2.83			
aug-cc-pVTZ CASSCF	−682.731578	−682.726666	3.08	2.89			
cc-pVDZ MRCI	−682.882814	−682.877507	3.33	3.13			
cc-pVTZ MRCI	−682.964468	−682.959187	3.31	3.11			
aug-cc-pVDZ MRCI	−682.897281	−682.892168	3.21	3.00			
aug-cc-pVTZ MRCI	−682.969841	−682.964526	3.34	3.13			
cc-pVDZ Mk-MRCCSD[b]	−682.887132	−682.881902	3.28				
cc-pVTZ Mk-MRCCSD	−682.974905	−682.969709	3.26				
cc-pVQZ Mk-MRCCSD	−683.000833	−682.995548	3.32				

[a] The active space is defined as (12e/10MO). [b] The active space for the reference wavefuntions is defined as (2e/2MO).

$$\Psi = 0.901\Phi_1[(\text{core})(5a_g)^2(5b_u)^2(6b_u)^2(6a_g)^2(7a_g)^2(2a_u)^2]$$
$$- 0.189\Phi_2[(\text{core})(5a_g)^2(5b_u)^2(6b_u)^2(6a_g)^2(7a_g)^2(2b_g)^2]$$
$$+ 0.063\Phi_3[(\text{core})(5a_g)^2(5b_u)^2(6b_u)^2(6a_g)^2(7a_g\alpha)(2a_u\beta)(2b_g\alpha)(7b_u\alpha)]$$
$$+ 0.050\Phi_4[(\text{core})(5a_g)^2(5b_u)^2(6b_u\beta)(6a_g\alpha)(7a_g)^2(2a_u)^2(8b_u\beta)(8a_g\alpha)]$$
$$+ 0.050\Phi_5[(\text{core})(5a_g)^2(5b_u)^2(6b_u)^2(6a_g)^2(7a_g\alpha)(2a_u\alpha)(2b_g\beta)(7b_u\beta)]$$
$$+ .....$$

Only the configuration state functions (CSFs) whose absolute CI coefficients are larger than 0.05 are shown. These confirm the predominantly single-reference nature of the trans isomer. The most dominant excited configuration present, denoted Φ_2, corresponds to a HOMO (in Figure 7a) to LUMO (in Figure 7b) double excitation, $[(2a_u)^2 \rightarrow (2b_g)^2]$. The aug-cc-pVTZ MRCI wave function for cis-HPPH is represented, in terms of natural orbitals, by

$$\Psi = 0.900\Phi_1[(\text{core})(5a_1)^2(5b_2)^2(6a_1)^2(7a_1)^2(6b_2)^2(2b_1)^2]$$
$$- 0.193\Phi_2[(\text{core})(5a_1)^2(5b_2)^2(6a_1)^2(7a_1)^2(6b_2)^2(2a_2)^2]$$
$$- 0.072\Phi_3[(\text{core})(5a_1)^2(5b_2)^2(6a_1)^2(7a_1\alpha)(6b_2)^2(2b_1\beta)(2a_2\beta)(7b_2\alpha)]$$
$$- 0.069\Phi_4[(\text{core})(5a_1)^2(5b_2)^2(6a_1)^2(7a_1\alpha)(6b_2)^2(2b_1\alpha)(2a_2\beta)(7b_2\beta)]$$
$$+ 0.057\Phi_5[(\text{core})(5a_1)^2(5b_2)^2(6a_1\alpha)(7a_1)^2(6b_2\beta)(2b_1)^2(8a_1\alpha)(8b_2\beta)]$$
$$- 0.056\Phi_6[(\text{core})(5a_1)^2(5b_2)^2(6a_1)^2(7a_1)^2(2b_1)^2(8a_1)^2]$$
$$- 0.052\Phi_7[(\text{core})(5a_1)^2(5b_2)^2(6a_1)^2(6b_2)^2(2b_1)^2(7b_2)^2]$$
$$+ .....$$

Again, the second CSF corresponds to a HOMO (in Figure 8a) to LUMO (in Figure 8b) double excitation, $[(2b_1)^2 \rightarrow (2a_2)^2]$, while the dominant configuration has a CI coefficient of 0.9, indicating only marginal multireference character.

Increasing the presence of electron correlation elongates both the P−P and P−H bond lengths in all three of these isomers (in Figures 2−4), which is consistent with the extra antibonding character introduced into the correlated wave function. The PPH_2 structure presents the shortest P−P bond length, while the cis-HPPH has the longest. The similar trend is observed among the H−P bond lengths, with PPH_2 possessing the shortest out of the three minima investigated here. The H−P bond lengths in the cis- and trans-HPPH structures are nearly equal, but slightly shorter in the cis isomer. At the CISD, CCSD, and CCSD(T) levels of theory, the HPP bond angles of trans and cis structures decrease compared with the SCF predictions. However, with the application of correlated methods, the PPH bond angle in the PPH_2 structure increases gradually. The (12e/10MO) CASSCF and MRCI methods seem to overestimate the bond lengths and bond angles of trans and cis structures compared to the more reliable CCSD and CCSD(T) methods.

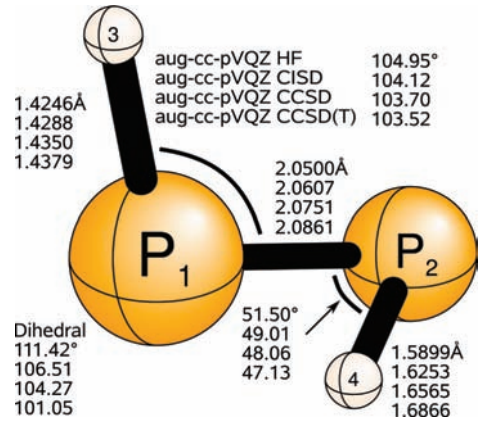

Figure 5. Theoretical geometries for the isomerization transition state linking trans-HPPH and planar PPH_2.

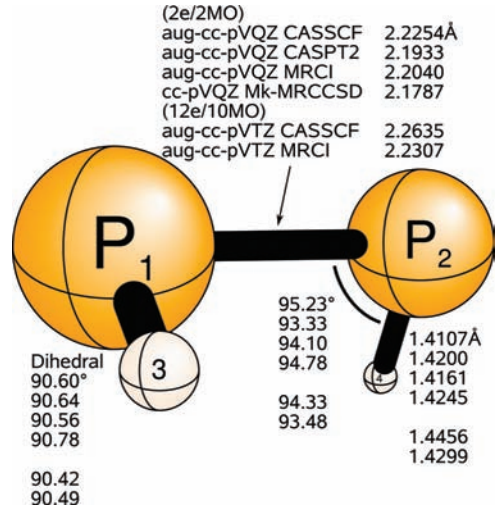

Figure 6. Theoretical geometries for the isomerization transition state linking trans-HPPH and cis-HPPH.

In contrast, at the (2e/2MO) Mk-MRCCSD level of theory, the bond angles and bond lengths are consistent with the CCSD prediction. This further proves that these isomers only possess little multireference character.

With the aug-cc-pVQZ CCSD(T) method, the magnitudes of the dipole moments for trans-HPPH, cis-HPPH, and PPH_2 are 0 (by symmetry), 1.1, and 2.3 D, respectively (in Tables 1−3). The planar PPH_2 isomer exhibits a larger dipole moment than the cis isomer, whose C_2 axis is perpendicular to the PP bond. This is expected, given that the PPH_2 isomer is more extended along the C_2 axis, which is defined by the PP bond. The orientation of the C_2 axes in these systems gives rise to dipole moments that are parallel to the PP bond in planar PPH_2, but perpendicular in cis-HPPH.

The harmonic vibrational frequencies of these structures (in Tables 1−3) decrease by about 100 cm^{-1} proceeding from SCF to CCSD(T); consequently, the zero-point vibrational energy (ZPVE) decreases with a more complete description of correlation effects. This behavior is symptomatic of reduced force constants, which result from the extra antibonding character in the correlated wave functions. The harmonic vibrational frequencies in the trans- and cis-HPPH structures from the treatment of (12e/10MO) CASSCF and MRCI are in reasonable agreement with the other levels of theory used.

The asymmetric PH stretching mode (ω_5) of trans-HPPH (in Table 1) presents the strongest infrared (IR) intensity, which is about an order of magnitude larger than the asymmetric bending

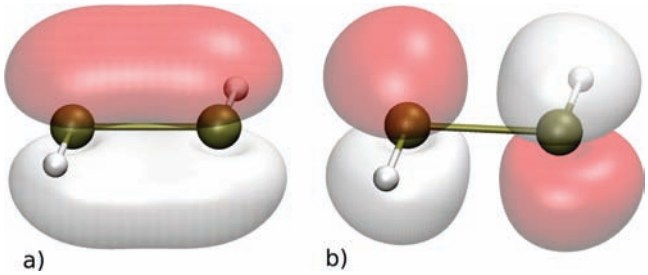

Figure 7. The $2a_u$ (HOMO) (a) and $2b_g$ (LUMO) (b) molecular orbitals for ^1A_g trans-HPPH at the cc-pVTZ SCF level of theory.

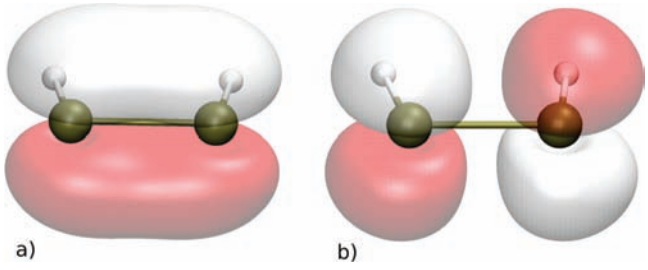

Figure 8. The $2b_1$ (HOMO) (a) and $2a_2$ (LUMO) (b) molecular orbitals for $^1A_1$ cis-HPPH at the cc-pVTZ SCF level of theory.

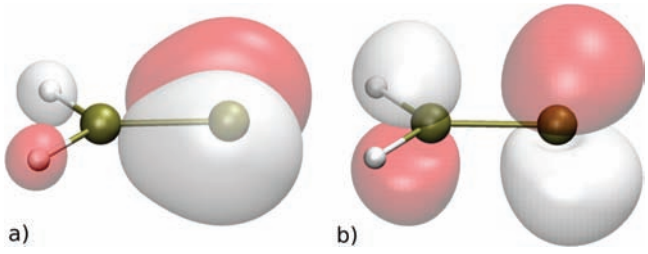

Figure 9. The $4b_2$ (HOMO) (a) and $4b_1$ (LUMO) (b) molecular orbitals for $^1A_1$ planar PPH_2 at the cc-pVTZ SCF level of theory.

(ω_6). However, the intensities for the other vibrational frequencies are zero by symmetry; the intensity for the torsion mode (ω_4) is almost equal to zero although it is allowed according to IR selection rules. In the cis-HPPH isomer (in Table 2), the most intense vibrational mode originates from the symmetric PH stretching mode (ω_1), while the PP stretching mode (ω_3) is the weakest IR active mode. As observed for the vibrational frequencies, the (12e/10MO) CASSCF and MRCI methods provide IR intensities that are in reasonable accord with coupled cluster theory. The IR intensities computed for the vibrational modes of PPH_2 (in Table 3) are comparable to those for trans-HPPH and cis-HPPH, exhibiting only a slight dependence on the level of theory employed.

As shown in Table 4, the classical energetic difference between trans- and cis-HPPH isomers is predicted to be 3.5 (SCF), 3.5 (CISD), 3.4 (CCSD), and 3.4 kcal mol^{-1} [CCSD(T)] with the aug-cc-pVQZ basis set. Multireference treatments predict slightly smaller differences of 3.1 [(12e/10MO)(CASSCF)], 3.3 kcal mol^{-1} (MRCI) with the aug-cc-pVTZ basis set, and 3.3 kcal mol^{-1} [(2e/2MO)(Mk-MRCCSD)] with cc-pVQZ basis set. Employing our most reliable method, aug-cc-pVQZ CCSD(T), the final ZPVE-corrected trans-cis energy gap is predicted to be 3.2 kcal mol^{-1}.

The energy difference between trans-HPPH and the planar PPH_2 structure is estimated to fall within the range of 24.2−26.2 kcal mol^{-1}. With the more complete treatment of electron correlation effects, the difference increases gradually. At our most reliable level of theory, aug-cc-pVQZ CCSD(T), the ZPVE-corrected energy gap is predicted to be 25.2 kcal mol^{-1}.

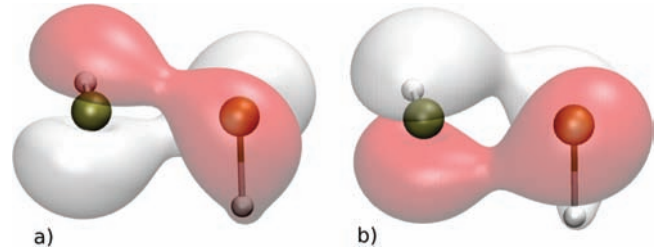

Figure 10. The 9a (a) and 8b (b) molecular orbitals for the isomerization transition state between trans-HPPH and cis-HPPH at the cc-pVTZ CASSCF level of theory.

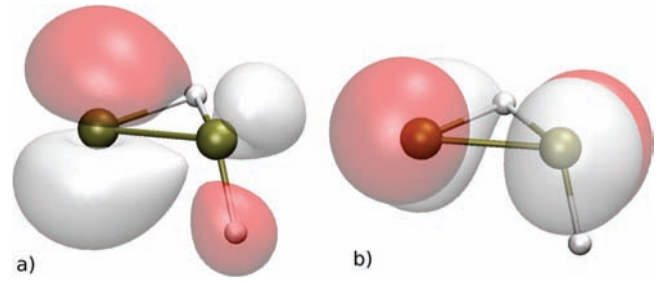

Figure 11. The HOMO (a) and LUMO (b) for the isomerization transition state (1,2 hydrogen shift) between trans-HPPH and planar PPH_2 at the cc-pVTZ SCF level of theory.

Transition States. In Figures 5 and 6, the representative optimized structures of the two isomerization transition states are depicted. The harmonic vibrational frequencies and dipole moments are shown in Tables 5 and 6. In Table 7, the total energies and ZPVE-corrected energies for the transition states are reported.

The 1,2 hydrogen shift in similar model systems (SCH_2, NPH_2, and PPH_2) demonstrates two different transition states, an in-plane transition state with C_s symmetry or out-of-plane transition state with C_1 symmetry.[67] However, as for PPH_2 the in-plane stationary point possesses more than one imaginary frequencies (a second-order saddle point) and higher energy barrier. Nguyen and Ha suggested that the migrating hydrogen behaves as a proton in the out-of-plane transition state between trans-HPPH and planar PPH_2.[67] The $P_2P_1H_3$ bond angle at the transition state is about 104°, as shown in Figure 5, which is larger than that of the trans structure (94°), but smaller than for the planar PPH_2 structure (128°). The $P_1P_2H_4$ bond angle is about 47°, which is roughly half of that of the trans structure. This indicates that the H_4 proton moves above the PP bond, forming a 3-center bond. Moreover, the $H_3P_1P_2H_4$ dihedral angle, which is about 101°, demonstrates that the 3-center bonding involves the P_1H_3 bond as well. It should be noted that the dihedral angle is sensitive to degree of correlation and is about 10° smaller at the CCSD(T) level of theory than at the SCF level. Using the P_2H_4 bond length as a measure of the reaction progress, an later transition state, that is, one that more closely resembles PPH_2, is predicted with increasing correlation. These trends are mirrored by the relative energies of the trans-HPPH and planar PPH_2 species in Table 4 with a later transition state correlating with a more endothermic reaction in keeping with the Hammond postulate.[68]

The harmonic vibrational frequencies of this isomerization transition state are shown in Table 5. The magnitude of the imaginary vibrational frequency decreases by about 370 cm^{-1} going from SCF to CCSD(T), showing a large dependence upon the theoretical model used. The imaginary vibrational frequency decreases with increasing basis set size as well. Despite the high sensitivity of the imaginary frequency, the real vibrational frequencies are less sensitive to the level of theory. The dipole moment

TABLE 5: Theoretical Prediction of Harmonic Vibrational Frequencies (in cm^{-1}), ZPVE (in kcal mol^{-1}), and Dipole Moments (μ_e, in Debye) for the Isomerization Transition State between the trans-HPPH and Planar PPH_2 Structures

theory	μ_e	ω_1(a)	ω_2(a)	ω_3(a)	ω_4(a)	ω_5(a)	ω_6(a)	ZPVE
aug-cc-pVTZ HF	1.44	2372	1777	1094	894	626	1154i	9.67
aug-cc-pVQZ HF	1.43	2373	1781	1101	899	629	1148i	9.70
cc-pVTZ CISD[a]		2308	1777	1084	854	590	975i	9.45
cc-pVQZ CISD		2317	1788	1083	860	600	951i	9.50
aug-cc-pVTZ CISD		2311	1771	1078	850	588	964i	9.43
aug-cc-pVQZ CISD		2317	1786	1082	859	599	949i	9.50
cc-pVTZ CCSD	1.25	2253	1766	1004	830	562	912i	9.17
cc-pVQZ CCSD	1.27	2261	1776	1002	836	573	885i	9.22
aug-cc-pVTZ CCSD	1.26	2256	1756	997	826	560	899i	9.14
aug-cc-pVQZ CCSD	1.26	2261	1773	1000	835	571	881i	9.21
cc-pVTZ CCSD(T)	1.23	2226	1791	922	812	541	821i	9.00
cc-pVQZ CCSD(T)	1.25	2234	1800	914	817	552	781i	9.03
aug-cc-pVTZ CCSD(T)	1.25	2229	1779	913	808	538	803i	8.96
aug-cc-pVQZ CCSD(T)[b]		2233	1795	912	817	550	775i	9.02

[a] The algorithm used to compute the CISD energies did not afford dipole moments. [b] The aug-cc-pVQZ CCSD(T) vibrational frequencies were computed using numerical differentiation of energies, which did not afford dipole moments.

TABLE 6: Theoretical Prediction of Harmonic Vibrational Frequencies (in cm^{-1}), ZPVE (in kcal mol^{-1}), and Dipole Moments (μ_e, in Debye) for the Isomerization Transition State between the trans- and cis-HPPH Structures

theory	μ_e	ω_1(a)	ω_2(a)	ω_3(a)	ω_4(a)	ω_5(b)	ω_6(b)	ZPVE
			(2e/2MO)					
cc-pVTZ CASSCF	0.832	2485	781	464	982i	2484	784	10.01
cc-pVQZ CASSCF	0.832	2489	784	465	1002i	2488	785	10.02
aug-cc-pVTZ CASSCF	0.835	2487	781	465	992i	2486	783	10.01
aug-cc-pVQZ CASSCF	0.831	2489	784	465	1004i	2488	785	10.02
cc-pVTZ MRCI	0.780	2418	732	454	1091i	2418	736	9.66
cc-pVQZ MRCI	0.786	2428	737	461	1137i	2427	740	9.71
aug-cc-pVTZ MRCI	0.768	2417	733	454	1107i	2417	736	9.66
aug-cc-pVQZ MRCI	0.780	2427	737	460	1142i	2426	740	9.71
cc-pVTZ CASPT2	0.799	2401	702	456	1052i	2401	705	9.53
cc-pVQZ CASPT2	0.800	2403	705	460	1081i	2404	707	9.55
aug-cc-pVTZ CASPT2	0.796	2395	702	454	1064i	2396	705	9.51
aug-cc-pVQZ CASPT2	0.796	2400	704	459	1086i	2401	707	9.54
cc-pVDZ Mk-MRCCSD		2331	707	447	1045i	2331	714	9.34
cc-pVTZ Mk-MRCCSD		2339	704	464	1132i	2339	701	9.36
			(12e/10MO)					
cc-pVDZ CASSCF	0.870	2205	701	388	1044i	2206	708	8.87
cc-pVTZ CASSCF	0.802	2204	705	400	1127i	2206	709	8.90
aug-cc-pVDZ CASSCF	0.802	2205	701	392	1093i	2207	706	8.88
aug-cc-pVTZ CASSCF	0.796	2207	705	400	1144i	2209	708	8.91
cc-pVDZ MRCI	0.771	2300	698	404	1034i	2300	706	9.16
cc-pVTZ MRCI	0.748	2305	698	425	1152i	2306	703	9.20
aug-cc-pVDZ MRCI	0.686	2288	692	403	1078i	2288	699	9.11
aug-cc-pVTZ MRCI	0.727	2303	699	425	1174i	2305	703	9.20

for this transition state is determined to be 1.25 D with CCSD(T), as shown in Table 5. At the aug-cc-pVQZ CCSD(T) level of theory, the trans-HPPH→ PPH_2 isomerization barrier is predicted to be 50.3 kcal mol^{-1}, which drops to 48.2 kcal mol^{-1} upon inclusion of ZPVE corrections (in Table 7). This is 3.2 kcal mol^{-1} lower than the barrier height of 51.4 kcal mol^{-1} determined by Nguyen using MP4/6-311++G (df,p).[67] At the aug-cc-pVQZ CCSD(T) level of theory, the barrier for the reverse process, PPH_2 → trans-HPPH is determined to be 23.0 kcal mol^{-1}.

Conversion between trans- and cis-HPPH may occur either by internal rotation about the P−P bond or through a structure with a linear P−P−H bond ("inversion"). It has previously been shown[28] that the rotational reaction path exhibits a much lower reaction barrier. During the rotational reaction path, the molecule possesses C_2 symmetry. However, the trans and cis structures have different orbital occupation in the C_2 subgroup [trans, $(9a^2 7b^2)$; cis, $(8a^2 8b^2)$]. Consequently, this process is forbidden according to Woodward−Hoffmann rules, and multireference methods are required to properly describe the transition state. Here, CASSCF and MRCI, each with two different defined active spaces (2e/2MO and 12e/10MO) are applied to characterize the transition state. In addition, (2e/2MO) CASPT2 and (2e/2MO) Mk-MRCCSD are also employed to characterize the transition state. The aug-cc-pVTZ CASSCF (2e/2MO) wave function for the transition state is represented, in terms of natural orbitals, by

$$\Psi = 0.708\Phi_1[(\text{core})(6a)^2(6b)^2(7a)^2(7b)^2(8a)^2(9a)^2] - 0.705\Phi_2[(\text{core})(6a)^2(6b)^2(7a)^2(7b)^2(8a)^2(8b)^2] + \ldots\ldots\ldots\ldots$$

and at the corresponding MRCI level it is

$$\Psi = 0.663\Phi_1[(\text{core})(6a)^2(6b)^2(7a)^2(7b)^2(8a)^2(9a)^2] - 0.659\Phi_2[(\text{core})(6a)^2(6b)^2(7a)^2(7b)^2(8a)^2(8b)^2] + \ldots\ldots\ldots\ldots$$

TABLE 7: Theoretical Predictions of the Total Energies (in E_h) for the Isomerization Reactions (Relative Energies (ΔE_e) and ZPVE-Corrected Relative Energies (ΔE_0) Are in kcal mol^{-1} With Respect to the trans-HPPH Closed-Shell Structure Obtained by the Same Method and Basis Set

	^1A_g trans-HPPH	transition state connecting trans-HPPH and planar PPH_2			transition state connecting trans-HPPH and cis-HPPH		
theory	energy	energy	ΔE_e	ΔE_0	energy	ΔE_e	ΔE_0
aug-cc-pVTZ HF	−682.643184	−682.562425	50.68	48.44			
aug-cc-pVQZ HF	−682.650899	−682.570127	50.69	48.46			
cc-pVTZ CISD	−682.936526	−682.856358	50.31	48.24			
cc-pVQZ CISD	−682.960652	−682.880883	50.06	47.99			
aug-cc-pVTZ CISD	−682.941826	−682.862282	49.91	47.84			
aug-cc-pVQZ CISD	−682.962771	682.883196	49.93	47.86			
cc-pVTZ CCSD	−682.972302	−682.892356	50.17	48.11			
cc-pVQZ CCSD	−682.998244	−682.918799	49.85	47.79			
aug-cc-pVTZ CCSD	−682.978383	−682.899205	49.69	47.62			
aug-cc-pVQZ CCSD	−683.000584	−682.921380	49.70	47.63			
cc-pVTZ CCSD(T)	−682.991391	−682.910189	50.95	48.90			
cc-pVQZ CCSD(T)	−683.019299	−682.938821	50.50	48.43			
aug-cc-pVTZ CCSD(T)	−682.998344	−682.918093	50.36	48.29			
aug-cc-pVQZ CCSD(T)	−683.021992	−682.941811	50.31	48.23			
cc-pVDZ CASSCF[a]	−682.704374				−682.651100	33.43	31.66
cc-pVTZ CASSCF	−682.730516				−682.675189	34.72	32.97
aug-cc-pVDZ CASSCF	−682.708350				−682.654713	33.66	31.92
aug-cc-pVTZ CASSCF	−682.731578				−682.676062	34.84	33.09
cc-pVDZ MRCI	−682.882814				−682.830555	32.79	31.01
cc-pVTZ MRCI	−682.964468				−682.908903	34.87	33.11
aug-cc-pVDZ MRCI	−682.897281				−682.844974	32.82	31.07
aug-cc-pVTZ MRCI	−682.969841				−682.913988	35.05	33.29
cc-pVDZ Mk-MRCCSD[b]	−682.881732				−682.835028	32.70	
cc-pVTZ Mk-MRCCSD	−682.974905				−682.920341	34.24	
cc-pVQZ Mk-MRCCSD	−682.000833				−682.944749	35.19	

[a] The active space is defined as (12e/10MO). [b] The active space for the reference wave functions is defined as (2e/2MO).

and the analogous CASPT2 method gives

$$\begin{aligned}\Psi &= 0.709\Phi_1[(\text{core})(6a)^2(6b)^2(7a)^2(7b)^2(8a)^2(9a)^2] \\ &- 0.704\Phi_2[(\text{core})(6a)^2(6b)^2(7a)^2(7b)^2(8a)^2(8b)^2] \\ &+ \text{.....}\end{aligned}$$

The above wave functions are composed of two CSFs with almost equal CI coefficients. We would expect these two configurations to provide a faithful description of the system; this is corroborated by the multireference computations employing a larger active space (full valence, 12e/10MO). The aug-cc-pVTZ MRCI wave function of the transition state is described, in terms of natural orbitals, by

$$\begin{aligned}\Psi &= 0.652\Phi_1[(\text{core})(6a)^2(6b)^2(7a)^2(7b)^2(8a)^2(9a)^2] \\ &- 0.648\Phi_2[(\text{core})(6a)^2(6b)^2(7a)^2(7b)^2(8a)^2(8b)^2] \\ &+ 0.058\Phi_3[(\text{core})(6a)^2(6b)^2(7b)^2(7a)^2(8a\alpha)(9a\beta) \\ &\qquad (8b\alpha)(9b\beta)] \\ &- 0.057\Phi_4[(\text{core})(6a)^2(6b)^2(7b)^2(7a)^2(9a)^2(9b)^2] \\ &+ 0.057\Phi_5[(\text{core})(6a)^2(6b)^2(7b)^2(7a)^2(8b)^2(9b)^2] \\ &+ \text{.....}\end{aligned}$$

The two CSFs $[(9a)^2(7b)^2$ and $(8a)^2(8b)^2]$ whose coefficients are greater than 0.6 are the same as those in the smaller active space (2e/2MO) computations. This indicates that a (2e/2MO) active space may be sufficient to describe the transition state, particularly if dynamical correlation is added through MRCI, CASPT2, or Mk-MRCCSD.

The PP bond length (in Figure 6) at the trans-cis transition state significantly increases because the alignment of p orbitals is no longer forming a π-bond. The bond order drops to one, that is, only one σ-bond is left. At the transition state, the dihedral angle is almost 90°, which indicates that the transition state lies about half way between reactant and product; this is expected given the small energy difference between trans-HPPH and cis-HPPH (in Table 4). All of the methods predict a similar structure; however, most of the real frequencies, shown in Table 6, decrease by roughly 100 cm^{-1} from (2e/2MO) CASSCF to (2e/2MO) Mk-MRCCSD due to the additional dynamical correlation. In contrast, the imaginary frequency increases with additional dynamical correlation. Furthermore, the dipole moment is predicted to be 0.8 D, which is intermediate between the trans- and cis-HPPH structures. The trans-cis isomerization barrier is estimated to be 35.2 kcal mol^{-1} (in Table 7) using our most reliable level of theory, (2e/2MO) Mk-MRCCSD with the cc-pVQZ basis set. This is significantly lower than the barrier from trans-HPPH to planar PPH_2.

Attempts to synthesize phosphenes have typically employed bulky substituent groups to prevent oligomerization; matrix isolation should, in principle, also achieve this. However, in isolation, unimolecular isomerization is still possible. Using the standard transistion state theory (TST) reaction rate[69]

$$k(T) = \left(\frac{k_B T}{h}\right)\frac{Q^{\ddagger}}{Q}e^{-E_0/k_B T} \qquad (1)$$

where the partition functions for trans-HPPH (Q) and the transition states ($Q^{\ddagger}$) are evaluated using direct summation

over rigid rotor and harmonic oscillator energy levels, we can compute the rate of isomerization of trans-HPPH to both cis-HPPH and planar PPH_2. Even at a temperature as high as 298 K, we compute the rates for isomerization to [cis-HPPH, planar PPH_2] to be just [3×10^{-12}, 2×10^{-23}] s^{-1} at the [aug-cc-pVTZ MRCI, aug-cc-pVQZ CCSD(T)] levels of theory, which correspond to half-lives of [3×10^{11}, 4×10^{22}] s, respectively. If the same analysis is performed with our lowest levels of theory, [cc-pVDZ CASSCF, aug-cc-pVTZ SCF], the rates become [5×10^{-11}, 2×10^{-23}] s^{-1}, respectively, which confirms the insensitivity of the reaction rates to level of theory employed.

According to the simple Wigner tunnelling correction,[70] this rate is accelated by a factor of

$$k_W(T) = 1 + \frac{1}{24}\left(\frac{h\nu_i}{k_B T}\right) \quad (2)$$

where ν_i is the magnitude of the imaginary vibrational frequency connecting reactants and products. The values of k_W at 4 K are just [7433, 3241] for isomerization reactions to form [cis-HPPH, planar PPH_2] at the [aug-cc-pVTZ MRCI, aug-cc-pVQZ CCSD(T)] levels of theory. Given the sensitivity of the imaginary frequencies, we also computed the Wigner correction using [cc-pVDZ CASSCF, aug-cc-pVTZ SCF] vibrational frequencies at 4 K, resulting in classical rate increases by a factor of [5877, 7180]. These confirm that although the imaginary vibrational frequencies exhibit significant dependence upon the level of theory, the resulting tunnelling corrections, and hence the halflives, are of the same order of magnitude. The fact that these isomerization rates are so small, even at high temperatures, and that the tunnelling is not significant even at low temperatures bolsters the feasibility of experimentally characterizing trans-HPPH.

Concluding Remarks. Trans- and cis-HPPH diphosphene as well as planar PPH_2 diphosphinylidene have been studied using highly correlated ab initio electronic structure theory. Multireference wave functions were required to investigate the isomerization transition state between the trans and cis structures. The trans-cis isomerization transition state barrier is predicted to be 35.2 kcal mol^{-1} using the Mk-MRCCSD method. At the highest level of theory, aug-cc-pVTZ CCSD(T), the barrier for the isomerization transition state between trans-HPPH and planar PPH_2 is predicted to be 48.2 kcal mol^{-1}. The results for this unusual nonplanar transition state should be of aid in understanding the nature of 1,2 hydrogen shifts for phosphorus compounds involving the PP double bond.

Acknowledgment. T.L. thanks Dr. S. E. Wheeler for insightful discussions. This research was supported by the U.S. Department of Energy, Office of Basic Energy Sciences, Grant DE-FG02-00ER14748 and used resources of the National Energy Research Scientific Computing Center, which is supported by the Office of Science of the U.S. Department of Energy under Contract DE-AC02-05CH11231.

References and Notes

(1) Cowley, A. H. *Acc. Chem. Res.* **1984**, *17*, 386.
(2) Scherer, O. J. *Angew. Chem., Int. Ed.* **1990**, *29*, 1104.
(3) Klinkhammer, K. W. *Angew. Chem., Int. Ed.* **1997**, *36*, 2320.
(4) Power, P. P. *J. Chem. Soc., Dalton Trans.* **1998**, *18*, 2939.
(5) Robinson, G. H. *Acc. Chem. Res.* **1999**, *32*, 773.
(6) Power, P. P. *Chem. Rev.* **1999**, *99*, 3463.
(7) Grützmacher, H.; Fässler, T. F. *Chem.—Eur. J.* **2000**, *6*, 2317.
(8) Cowley, A. H. *Polyhedron* **1984**, *3*, 389.
(9) Geoffroy, M.; Jouaiti, A.; Terron, G.; Cattani-Lorente, M.; Ellinger, Y. *J. Phys. Chem.* **1992**, *96*, 8241.
(10) Binder, H.; Riegel, B.; Heckmann, G.; Moscherosch, M.; Kaim, W.; von Schnering, H.-G.; Hönle, W.; Flad, H.-J.; Savin, A. *Inorg. Chem.* **1996**, *35*, 2119.
(11) Kawasaki, S.; Nakamura, A.; Toyota, K.; Yoshifuji, M. *Bull. Chem. Soc. Jpn.* **2005**, *78*, 1110.
(12) Sasamori, T.; Tokitoh, N. *Dalton Trans.* **2008**, *11*, 1395.
(13) Matus, M. H.; Nguyen, M. T.; Dixon, D. A. *J. Phys. Chem. A* **2007**, *111*, 1726.
(14) Shah, S.; Concolino, T.; Rheingold, A. L.; Protasiewicz, J. D. *Inorg. Chem.* **2000**, *39*, 3860.
(15) Yoshifuji, M.; Shima, I.; Inamoto, N.; Hirotsu, K.; Higuchi, T. *J. Am. Chem. Soc.* **1981**, *103*, 4587.
(16) Cowley, A. H.; Decken, A.; Norman, N. C.; Krüger, C.; Lutz, F.; Jacobsen, H.; Ziegler, T. *J. Am. Chem. Soc.* **1997**, *119*, 3389.
(17) Yoshifuji, M. *J. Chem. Soc., Dalton Trans.* **1998**, *20*, 3343.
(18) Twamley, B.; Power, P. P. *Chem. Comm.* **1998**, *18*, 1979.
(19) Twamley, B.; Sofield, C. D.; Olmstead, M. M.; Power, P. P. *J. Am. Chem. Soc.* **1999**, *121*, 3357.
(20) Sasamori, T.; Takeda, N.; Tokitoh, N. *J. Phys. Org. Chem.* **2003**, *16*, 450.
(21) Mathey, F. *Angew. Chem., Int. Ed.* **2003**, *42*, 1578.
(22) Wang, Y.; Xie, Y.; Wei, P.; King, R. B.; Schaefer, H. F.; v, R; Schleyer, P.; Robinson, G. H. *J. Am. Chem. Soc.* **2008**, *130*, 14970.
(23) Weber, L. *Chem. Rev.* **1992**, *92*, 1839.
(24) Tokitoh, N. *J. Organomet. Chem.* **2000**, *611*, 217.
(25) Caminade, A.-M.; Verrier, M.; Ades, C.; Paillous, N.; Koenig, M. *J. Chem. Soc., Chem. Commun.* **1984**, *13*, 875.
(26) Hamaguchi, H.; Tasumi, M.; Yoshifuji, M.; Inamoto, N. *J. Am. Chem. Soc.* **1984**, *106*, 508.
(27) Trinquier, J. *J. Am. Chem. Soc.* **1982**, *104*, 6969.
(28) Allen, T. L.; Scheiner, A. C.; Yamaguchi, Y.; Schaefer, H. F. *J. Am. Chem. Soc.* **1986**, *24*, 7579.
(29) Nguyen, M. T. *Chem. Phys.* **1986**, *109*, 277.
(30) Ito, K.; Nagase, S. *Chem. Phys. Lett.* **1986**, *126*, 531.
(31) Nagase, S.; Suzuki, S.; Kurakake, T. *J. Chem. Soc., Chem. Commun.* **1990**, *23*, 1724.
(32) Allen, T. L.; Scheiner, A. C.; Schaefer, H. F. *J. Phys. Chem.* **1990**, *94*, 7780.
(33) Jin, S.; Colegrove, B. T.; Schaefer, H. F. *Inorg. Chem.* **1991**, *30*, 2969.
(34) Mahé, L.; Barthelat, J.-C. *J. Phys. Chem.* **1995**, *99*, 6819.
(35) Cheng, H.-M.; Lin, C.-F.; Chu, S.-Y. *J. Phys. Chem. A* **2007**, *111*, 6890.
(36) Amatatsu, Y. *J. Phys. Chem. A* **2008**, *112*, 8824.
(37) Olkowska-Oetzel, J.; Pikies, J. *Appl. Organomet. Chem.* **2003**, *17*, 28.
(38) Nguyen, M. T.; van Keer, A.; Vanquickenborne, L. G. *J. Org. Chem.* **1996**, *61*, 7077.
(39) Kim, K.; Shavitt, I.; Del Bene, J. E. *J. Chem. Phys.* **1992**, *96*, 7573.
(40) Wetmore, R. W.; Schaefer, H. F. *J. Chem. Phys.* **1978**, *69*, 1648.
(41) Dunning, T. H. *J. Chem. Phys.* **1989**, *90*, 1007.
(42) Woon, D. E.; Dunning, T. H. *J. Chem. Phys.* **1993**, *98*, 1358.
(43) Brooks, B. R.; Laidig, W. D.; Saxe, P.; Goddard, J. D.; Yamaguchi, Y.; Schaefer, H. F. *J. Chem. Phys.* **1980**, *72*, 4652.
(44) Osamura, Y.; Yamaguchi, Y.; Schaefer, H. F. *J. Chem. Phys.* **1982**, *77*, 383.
(45) Rice, J. E.; Amos, R. D.; Handy, N. C.; Lee, T. J.; Schaefer, H. F. *J. Chem. Phys.* **1986**, *85*, 963.
(46) Hampel, C.; Peterson, K. A.; Werner, H.-J. *Chem. Phys. Lett.* **1992**, *190*, 1.
(47) Watts, J. D.; Gauss, J.; Bartlett, R. J. *Chem. Phys. Lett.* **1992**, *200*, 1.
(48) Raghavachari, K.; Trucks, G. W.; Pople, J. A.; Head-Gordon, M. *Chem. Phys. Lett.* **1989**, *157*, 479.
(49) Watts, J. D.; Gauss, J.; Bartlett, R. J. *J. Chem. Phys.* **1993**, *98*, 8718.
(50) Stanton, J. F. *Chem. Phys. Lett.* **1997**, *281*, 130.
(51) Knowles, P. J.; Werner, H.-J. *Chem. Phys. Lett.* **1985**, *115*, 259.
(52) Werner, H.-J.; Knowles, P. J. *J. Chem. Phys.* **1985**, *82*, 5053.
(53) Knowles, P. J.; Werner, H.-J. *Chem. Phys. Lett.* **1988**, *145*, 514.
(54) Werner, H.-J.; Knowles, P. J. *J. Chem. Phys.* **1988**, *89*, 5803.
(55) Roos, B. O.; Linse, P.; Siegbahn, P. E. M.; Blomberg, M. R. A. *Chem. Phys.* **1982**, *66*, 197.
(56) Andersson, K.; Malmqvist, P. Å.; Roos, B. O.; Sadlej, A. J.; Wolinski, K. *J. Phys. Chem.* **1990**, *94*, 5483.
(57) Andersson, K.; Malmqvist, P. Å.; Roos, B. O. *J. Chem. Phys.* **1992**, *96*, 1218.
(58) Mahapatra, U. S.; Datta, B.; Mukherjee, D. *Mol. Phys.* **1998**, *94*, 157.

(59) Evangelista, F. A.; Allen, W. D.; Schaefer, H. F. *J. Chem. Phys.* **2006**, *125*, 154113.

(60) Evangelista, F. A.; Allen, W. D.; Schaefer, H. F. *J. Chem. Phys.* **2007**, *127*, 024102.

(61) Werner, H.-J. et al. *MOLPRO*, version 2006.1 (a package of ab initio programs); see http://www.molpro.net.

(62) Stanton, J. F.; Gauss, J.; Watts, J. D.; Szalay, P. G.; Bartlett, R. J.; Auer, A. A.; Bernholdt, D. E.; Christiansen, O.; Harding, M. E.; Heckert, M.; Heun, O.; Huber, C.; Jonsson, D.; Jusélius, J.; Lauderdale, W. J.; Metzroth, T.; Michauk, C.; O'Neill, D. P.; Price, D. R.; Ruud, K.; Schiffmann, F.; Tajti, A.; Varner, M. E.; Vázquez, J. and the integral packages: *MOLECULE* (Almlöf, J. Taylor, P. R.), *Props* (Taylor, P. R.), and *Abacus* (Helgaker, T. Aa; Jensen, H. J.; Jørgensen, P.; Olsen, J.). For current version, see http://www.aces2.de.

(63) Stanton, J. F.; Gauss, J.; Watts, J. D.; Lauderdale, W. J.; Bartlett, R. J. *Int. J. Quantum Chem.* **1992**, *44* (S26), 879.

(64) Crawford, T. D.; Sherrill, C. D.; Valeev, E. F.; Fermann, J. T.; King, R. A.; Leininger, M. L.; Brown, S. T.; Janssen, C. L.; Seidl, E. T.; Kenny, J. P.; Allen, W. D. *J. Comput. Chem.* **2007**, *28*, 1610.

(65) Evangelista, F. A. *MCSCF* (program for multiconfiguration self-consistent field calculations); 2008.

(66) Evangelista, F. A.; Simmonett, A. C. *PSIMRCC* (computer code written at the University of Georgia to perform multireference coupled cluster computations); 2007; see http://www.ccc.uga.edu/psimrcc.

(67) Nguyen, M. T.; Ha, T.-K. *Chem. Phys. Lett.* **1989**, *158*, 135.

(68) Hammond, G. S. *J. Am. Chem. Soc.* **1953**, *77*, 334.

(69) Levine, R. D. *Molecular Reaction Dynamics*; Cambridge University Press: Cambridge, UK, 2005.

(70) Wigner, E. *Z. Phys. Chem. B* **1932**, *19*, 203.

JP904028A